Electroosmotic shear flow in microchannels

Dileep Mampallil and Dirk van den Ende*

Physics of Complex Fluids, MESA+ Institute, Dept. of Science and Technology

University of Twente, P.O. Box 217, 7500 AE Enschede, The Netherlands

July 19, 2012

Abstract

We generate and study electroosmotic shear flow in micro channels. By chemically or electrically modifying the surface potential of the channel walls a shear flow component with controllable velocity gradient can be added to the electroosmotic flow caused by double layer effects at the channel walls. Chemical modification is obtained by treating the channel wall with a cationic polymer. In case of electric modification, we used gate electrodes embedded in the channel wall. By applying a voltage to the gate electrode, the zeta potential can be varied and a controllable, uniform shear stress can be applied to the liquid in the channel. The strength of the shear stress depends on both the gate voltage and the applied field which drives the electroosmotic shear flow. Although the stress range is still limited, such a microchannel device can be used in principle as an in situ micro-rheometer for lab on a chip purposes.

Keywords: Electroosmotic flow, gate electrodes, shear flow, micro rheometer

---

*Corresponding author; electronic address: h.t.m.vandenEnde@tnw.utwente.nl

1 Introduction

Microfluidic devices are used for chemical analysis of biological fluids or other soft materials [1]. In several applications also knowledge of the rheological properties of such fluids is important in order to characterize them properly, for instance in medical diagnostics. Steady or oscillatory shear flow can be used to measure the rheological properties of fluids or to manipulate soft materials in microchannels. It can be used, for example, to stretch DNA molecules [2], to induce conformational changes in proteins [3], or to study the response of cells [4, 5]. Moreover, shear flow in micro channels can be used to study the rheology of complex fluids or colloids in confined flow [6, 7]. When sheared in confined geometries, colloidal suspensions can undergo several, shear-induced, configurational changes [8]. Under influence of electric fields the structure of colloidal gels can change, too [9]. When electric fields are not a drawback otherwise (for solutions containing biological material electric fields may be harmfull), electroosmotic flow (EOF) is a good option to create a shear flow in micro channels, because no moving mechanical parts are involved and controlling a gate voltage is from practical point of view straightforward. In particular solutions containing neutral or slightly charged polymers or colloidal particles can be examined in electroosmotic shear flow as a function of the particle or polymer concentration. Recently, several studies were reported connecting electrokinetics and rheology of complex fluids [10, 11, 12].

The magnitude and direction of electroosmotic flow depends on the applied electric field along the flow axis and on the surface charge or zeta potential at the channel wall [13]. When opposing walls are equally charged, EOF results in a plug flow profile. By changing the surface charge or the zeta potential, at one of the walls, this plug flow can be transformed to a shear flow. In this paper, we investigate the possibilities to modify the zeta potential at the channel wall chemically or electrically; in last case gate electrodes, embedded in the channel wall, are used. For most materials the intrinsic zeta potential is negative, but it can be decreased or even reversed to positive by coating the channel wall with a cationic polymer. This technique was first introduced in capillary electrophoresis to improve protein analyses [14] and is applied by several other authors [15, 16, 17, 18, 19]. Stroock *et al.* calculated, and verified experimentally, the flow profile in microchannels with oppositely charged surfaces [20]. To control the zeta potential with an external voltage, one can use gate electrodes which are embedded in the channel wall and covered with a dielectric layer to prevent direct electric contact with the fluid [21, 22, 23]. The potential applied at the gate electrode mainly drops over the dielectric layer but also partially over the Debye layer in the fluid. This results in an enhancement or reduction of the zeta potential depending on the sign of the applied potential compared to that of the intrinsic zeta potential. As a side effect, this local field enhancement may change under certain conditions the equilibrium between proton adsorption and desorption from the wall, which partially suppresses the change in zeta potential, thereby reducing the effect of the gate potential. For example, in a glass microchannel, the modification of the zeta potential by a gate potential is efficient at low pH of the electrolyte where the number of surface silanol groups is to low to create buffering effects [24], but is much less efficient at higher pH values. The principle of controlling the EOF by a gate potential has been used to enhance mixing effects [25], to modulate the concentration of ions and molecules in a nanochannel [26] or to perform titration in nano confinements [27]. To our best knowledge, this is the first time gate electrodes are used to generate a shear flow in a microchannel with the purpose to measure the rheological properties of the liquid in situ. We quantitatively describe the method to create a uniform shear flow and its theoretical background in section 2. In section 3 the experimental set-up and procedures have been presented. We present our experimental results in section 4 together with a discussion of the efficiency of such an approach and the shear rates that can be achieved in practice. Moreover, some practical issues are addressed, before we conclude our discussion in section 5.

2 Electroosmotic shear flow

2.1 General Flow profile

Let us consider a rectangular channel of length L, with the upper and bottom wall located at $y = \pm h/2$, while the width is $W \gg h$. This channel is filled with a $Z-Z$ electrolyte of which both components have a bulk number density n_0. A double layer is formed near the walls due to their surface charge. By applying an electric field E_∞ along the axial z direction, the mobile ions in the double layer are dragged by this field and an electroosmotic flow is generated. To understand this mechanism in more detail, we consider the potential in the channel, which is described by the Poisson equation:

$$\nabla^2\phi = \frac{-Ze}{\varepsilon_0\varepsilon_l}(n_+ - n_-) \tag{1}$$

where n_+ and n_- are the number density of positive and negative ions, e the fundamental charge, Z the valence of the ions, ε_0 is the permittivity of free space and ε_l the dielectric constant of the liquid. The electric force on an ion due to this potential, $\mp Ze\nabla\phi$, is balanced by the thermodynamic force, $-k_BT\nabla\ln(n_\pm/n_0)$, and the hydrodynamic force, $\zeta_\pm(\vec{v}_\pm - \vec{u})$, on the ion [28]

$$\mp Ze\nabla\phi - k_BT\nabla\ln(n_\pm/n_0) = \zeta_\pm(\vec{v}_\pm - \vec{u}) \tag{2}$$

where k_B is the Boltzmann constant, T the absolute temperature, $\zeta_\pm$ the friction coefficient of the ion, $\vec{v}_\pm$ its velocity and $\vec{u}$ the local fluid velocity. Assuming the flow is in the z direction only, the charge distribution, which only depends on the y coordinate, decouples from the flow field, so the y component of Eq. (2) can be solved to get:

$$n_\pm = n_0\exp\left(\mp\frac{Ze\psi}{k_BT}\right) \tag{3}$$

where ψ is the potential relative to the bulk potential at axial position z in the channel: $\psi(y,z) = \phi(y,z) + zE_\infty$. Assuming that ψ depends via its boundary conditions only weakly on z (i.e. $\partial^2\psi/\partial z^2 \ll \partial^2\psi/\partial y^2$) one obtains by substitution of Eq. (3) in Eq. (1):

$$\frac{\partial^2}{\partial y^2}\left(\frac{Ze\psi}{k_BT}\right) = \kappa^2\sinh\left(\frac{Ze\psi}{k_BT}\right) \tag{4}$$

with $\kappa = Ze[2n_0/(\varepsilon_0\varepsilon_l k_BT)]^{1/2}$ the inverse Debye length. In our experiments this length is much smaller than the height h of the channel, typically $\kappa h > 10^2 \gg 1$, in which case the solution of Eq. (4) is given by:

$$\phi(y,z) = 2\frac{k_BT}{Ze}\ln\left(\frac{1+A(y)+B(y)}{1-A(y)-B(y)}\right) - z\,E_\infty \tag{5}$$

with $A(y) = A_0e^{-\kappa h/2-\kappa y}$ and $B(y) = B_0e^{-\kappa h/2+\kappa y}$, where $A_0 = \tanh(Ze\psi_a/4k_BT)$ and $B_0 = \tanh(Ze\psi_b/4k_BT)$ are given by the relative potential at both walls: $\psi_a(z) = \psi(-h/2,z)$ and $\psi_b(z) = \psi(h/2,z)$.

To obtain the resulting flow profile inside the channel we consider the force balance on a fluid element with volume $dxdydz$ in the flow direction, which is given by:

$$\frac{\partial\tau}{\partial y} = \frac{\partial p}{\partial z} + \varepsilon_0\varepsilon_l\frac{\partial^2\phi}{\partial y^2}E_\infty \tag{6}$$

where τ is the shear stress in the liquid, $p(z)$ the pressure inside the channel and $eZ(n_+ - n_-) = -\varepsilon_0\varepsilon_l\,\partial^2\phi/\partial y^2$ the local charge density. By integrating Eq. (6) one obtains for the shear stress:

$$\tau(y) = \tau_0 + \frac{dp}{dz}y + \varepsilon_0\varepsilon_l E_\infty\frac{\partial\phi}{\partial y} \tag{7}$$

where $\partial\phi/\partial y$ is obtained from Eq. (5). Since $\partial\phi/\partial y$ is non-zero only in the double layer near the walls, the shear stress in absence of a pressure gradient will be constant over most of the channel cross section. This results in a homogeneous shear rate in the channel. Supposing the flow curve of the liquid under consideration is given by $\tau = \mathrm{f}(\dot\gamma)$ we obtain the differential equation for the velocity field:

$$\frac{du}{dy} = \mathrm{g}(\tau_0 + \frac{dp}{dz}y + \varepsilon_0\varepsilon_l E_\infty \frac{\partial\phi}{\partial y}) \tag{8}$$

where $\dot\gamma = \mathrm{g}(\tau)$ is the inverse function of $\tau = \mathrm{f}(\dot\gamma)$. In general Eq. (8) can be solved by numerical integration in which case the value for τ_0 should be optimized such that the resulting velocities at the walls become zero. In Appendix A we sketch a procedure to do so. For a Newtonian liquid with viscosity η this results in:

$$\dot\gamma_0 = \frac{u_b - u_a}{h} \tag{9}$$

$$\tau_0 = \varepsilon_0\varepsilon_l E_\infty \frac{\psi_a - \psi_b}{h} \tag{10}$$

with $u_{a,b} = -\varepsilon_0\varepsilon_l E_\infty \psi_{a,b}/\eta$ the velocity at the channel walls. $\dot\gamma_0$ and τ_0 are the rate of shear and the stress at the centerline of the channel. In an experiment, the velocity profiles $u(y)$ and so $\dot\gamma_0$ can be measured at different values of E_∞, for instance by particle tracking. Once the values for ψ_a and ψ_b are known, τ_0 can be calculated and the flow curve of the liquid is obtained from $\eta(\dot\gamma_0) = \tau_0/\dot\gamma_0$.

Because one has to determine first the values of ψ_a and ψ_b the technique is limited to measure only relative viscosities of, for example, colloidal particles dispersions or polymer solutions with a known solvent viscosity. In that case ψ_a and ψ_b can be determined for example, by the solution displacement method [29] using the solvent at the same ionic strength and pH as the dispersion or solution. Knowing the zeta potentials under the given conditions, the viscosity of the solution/dispersion can be measured relative to that of its solvent. Of course this approach only holds as long as the system experiences negligible adsorption effects from the particles or molecules in the test solution [10].

2.2 Channel with gate electrodes

2.2.1 A single electrode

To control the surface potential gate electrodes can be embedded in the channel wall. Charge injection will be prevented by covering these electrodes with a dielectric layer with thickness d and dielectric constant ε_d. When a potential V is applied to the gate electrode, it drops over both the dielectric layer and the Debye layer in the liquid to the bulk potential, as illustrated in Fig. 1. The boundary condition for the perpendicular component of the electric field at the channel wall is given by

$$\varepsilon_l E_2 - \varepsilon_d E_1 = \sigma/\varepsilon_0 \tag{11}$$

where E_1 is the field in the dielectric layer and $E_2 = -\partial\phi/\partial y$ is the field in the liquid, both perpendicular to the wall, while σ is the free charge on the liquid wall interface.

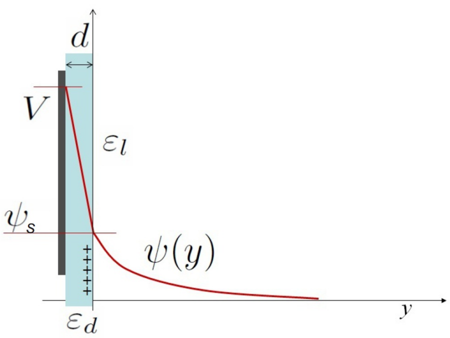

Figure 1: *Sketch of the electric potential near an electrode as a function of the penetration depth y.*

Using Eq. (5), Eq. (11) can be rewritten as:

$$\psi_s = \frac{q_s^{(0)}}{q_s + \varepsilon_d/(\kappa d \varepsilon_l)}\,\psi_s^{(0)} + \frac{\varepsilon_d/(\kappa d \varepsilon_l)}{q_s + \varepsilon_d/(\kappa d \varepsilon_l)}\,(V + zE_\infty) \tag{12}$$

Here $\psi(y) = \phi(y) + zE_\infty$ is the potential relative to the bulk potential at position z along the channel; ψ_s is the relative potential at the wall and $\psi_s^{(0)}$ the intrinsic potential at the wall due to the surface charge:

$$\sigma = \kappa \varepsilon_0 \varepsilon_l q_s^{(0)} \psi_s^{(0)} \tag{13}$$

with $q_s = q(Ze\psi_s/2k_BT)$ and $q_s^{(0)} = q(Ze\psi_s^{(0)}/2k_BT)$. The function $q(x)$ accounts for the correction of the Debye Hückel approximation in case $\psi_s \geq k_BT/Ze$:

$$q(x) = \frac{\sinh x}{x} \simeq 1 + \tfrac{1}{6}x^2 + ...$$

Hence the efficiency of the gate actuation depends on the ratio $\varepsilon_d/(\kappa d \varepsilon_l)$:

$$\frac{\partial \psi_s}{\partial V} \simeq \frac{\varepsilon_d}{\kappa d\, \varepsilon_l} \tag{14}$$

Taking $\varepsilon_d = 2$, $\varepsilon_l = 80$, $\kappa = 10^8$ m^{-1} and $d = 1$ μm we can adjust (in theory) the wall potential with the gate voltage by 0.25 mV/V.

2.2.2 An array of electrodes

From Eq. (12), it is clear that $\psi_s(z)$ varies along the electrode due to the potential gradient $-E_\infty$ in the channel. To minimize this effect, several electrodes with a width $w \ll L$ are embedded in the upper wall. We keep the relative potential at the electrodes $U_n = V_n + z_n E_\infty = U$ constant while $U_n \gg \Delta U_n = w\, E_\infty$, where z_n is the center position of electrode n. When the gate voltages V_n are applied, the surface potential ψ_b at the upper wall differs in the gate region from that between two gate electrodes, i.e. $\psi_b = \psi_s(z)$. This inhomogeneity leads to an axial variation of the driving force and hence (to ensure a homogeneous volumetric flow rate in the channel) produces a variation in the pressure gradient along the channel. To study this aspect in more detail, we consider a channel with length L, containing N electrodes with width w and spacing l between the electrodes, as illustrated in Fig. 2.

The volumetric flow rate,

$$\dot{Q} = Wh\,\langle u \rangle = Wh\left(\tfrac{1}{2}(u_a + u_s(z)) + u_p(z)\right) \tag{15}$$

should be constant. So the pressure gradient will vary as:

$$\partial_z p = \frac{-12\eta}{h^2} u_p = \frac{-12\eta}{h^2}\left(\langle u \rangle - \tfrac{1}{2}(u_a + u_s(z))\right) \tag{16}$$

where $u_s(z)$ along electrode n is given by:

$$\begin{aligned} u_s(z) &= -\frac{\varepsilon_0 \varepsilon_l E_\infty}{\eta} \psi_s(z) \\ &= -\frac{\varepsilon_0 \varepsilon_l E_\infty}{\eta q_s} \times \\ &\quad \left(q_s^{(0)} \, \psi_s^{(0)} + \varepsilon_d / (\kappa d \varepsilon_l) \left(U + (z - z_n) E_\infty \right) \right) \end{aligned} \tag{17}$$

while in between two electrodes $u_s(z)$ is equal to:

$$u_s(z) = -\frac{\varepsilon_0 \varepsilon_l E_\infty}{\eta} \psi_s^{(0)}$$

Due to this varying pressure contribution the flow profile inside the channel will vary with axial position. To minimize these variations, the ratio l/w as defined in Fig. 2 should be small while a constant potential difference between the gate electrode and the bulk fluid at that position should be maintained. This can be achieved with a resistor network as given in Fig. 2 (see also Appendix B).

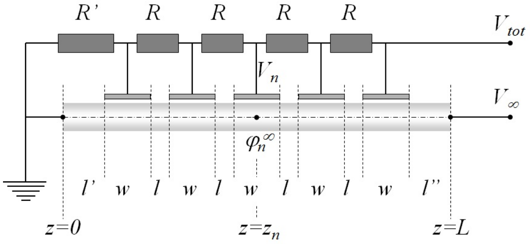

Figure 2: *Electric circuit with electrode connections.*

3 Experiments

3.1 Channel fabrication

The channel with the chemical modified surfaces was made of two flat borosilicate glass slides (Menzel–Glaser) separated by a para film as described in ref. [29]. To modify the surface charge, the glass slide was cleaned with detergent, isopropanol, and DI water and kept in 100 mM KOH at about 90°C for 30 minutes. After washing once more in DI water, the glass slides were kept in 3% HCl for at least one hour and again washed well in DI water. Next, the bottom glass slide was coated with solutions of 10% w/v Polybrene (PB), 3% w/v dextran sulfate (DS), and again 10% w/v PB by subsequently dipping it in the solutions for 10 minutes. After the first PB and DS coating the glass slide is rinsed in DI water for 1 minute. After the final PB coating, it was rinsed in DI water for at least 3 minutes to remove the excess PB from it. Last step is quite important because otherwise the excess PB will dissolve into the electrolyte in the channel and adsorb to the other walls thereby decreasing or even destroying the charge contrast and so the shear rate. The height of this channel (A) was 32 μm, as indicated in Fig. 3A.

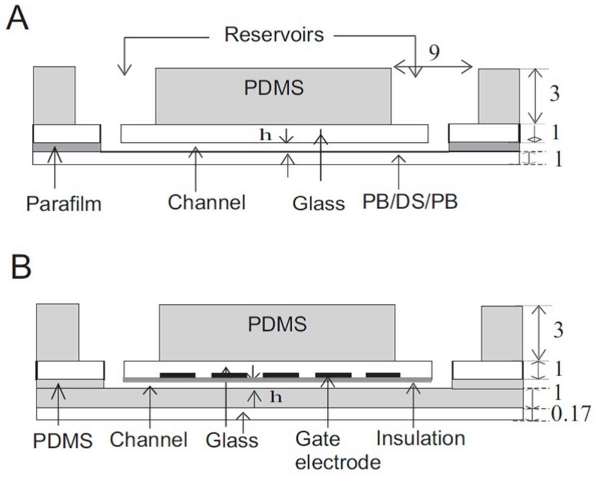

Figure 3: *Channel lay-out. Length (L), width (W) and height (H) of the channel A were 14 mm, 0.5 mm and 32 μm and those of channel B were 6 mm, 0.2 mm and 22 μm.*

In the second channel (B), gate electrodes have been embedded in the upper wall. These electrodes are of chromium-tungsten (Cr/W) films obtained by a lift off technique on borofloat glass. Each of the five electrodes is 600 μm in width and separated by 60 μm from its neighbors. The substrate containing the electrodes is coated with a $SiO_2/Si_3N_4/SiO_2$ trilayer (ONO layer) with a total thickness of 750 ±50 nm to insulate the electrode from the liquid. Finally, the substrate is annealed at 400 °C for 24 hours. The micro channel -with a height of 22 μm, a width of 200 μm and a length of 6 mm- is made of PDMS using soft lithography. The thickness of the PDMS block containing the channel is only 1 mm to allow for optical access of the channel via the PDMS side since the Cr/W electrodes are not transparent. A thin glass slide is kept under the PDMS block for mechanical support. The final channel lay-out is shown in Fig. 3B.

3.2 Measurements

As electrolyte solution, we used a pH 3 buffer (Fluka, cat no. 82565) dissolved in DI water consisting of 0.31 mM NaOH, 0.88 mM NaCl and 0.59 mM Citric acid, leading to a pH of 3.69 (measured 3.65) and an inverse Debye length $\kappa = 1.1 \times 10^8$ m^{-1}. The conductivity of the solution was 120 μS/cm. To visualize the flow we put polystyrene green fluorescent beads with a diameter of 0.43 μm as tracer particles in the electrolyte at a volume fraction of about 0.005%. The channel and both reservoirs are filled with the solution to the same height, preventing a pressure drop along the channel. The motion of the tracer particles was recorded using a Nikon Eclipse inverted microscope with 60 X objective and equipped with a camera (Photron fastcam Ultima 512). The frame rate was 60 or 125 frames per second depending on the speed of the particles. The low intensity of the images at higher frame rates limits the maximum field strength at which the EOF can be recorded. While the camera is recording, the channel is scanned along its height by shifting the focal plane of the objective at 2 μm/s using a piezo element (PI, E-662 LVPZT Position Servo Controller). All experiments were carried out at room temperature (22°C).

In channel A, the flow was recorded while varying the electric field, E_∞ from 3.5 to 10.7 V/mm. In channel B, the driving field was varied from 2.5 to 12.5 V/mm at a gate voltage, V_G of 500 V. Moreover, the gate voltage was varied from 0 to 500 V at a fixed driving field strength of 5 V/mm. During these measurements, the variable resistance R' was adjusted such that a constant potential difference was obtained between every gate electrode and the fluid near the centerline of the channel at the position of the electrode.

The recorded images of the flow field in each focal plane were analyzed using imageJ with a particle tracking algorithm [30]. Next, the particle trajectories generated with ImageJ are analyzed with a home made Matlab code to extract the velocity of each detected particle. The depth of view for the objective used is 1.2 μm, leading to an inaccuracy in the measured velocity of less than 5% for both channels. Finally these velocities are averaged. The obtained average particle velocity is the sum of the electrophoretic velocity $m_{\mathrm{EF}} E_\infty$ and the electroosmotic velocity $m_{\mathrm{EO}} E_\infty$. The electroosmotic mobility m_{EO} can be calculated knowing the electrophoretic mobility m_{EF} which is measured separately as $(-46 \pm 2) \times 10^{-9}$ m^2/Vs using a ZetaSizer (Malvern) for the used electrolyte solution.

4 Results and discussion

4.1 Chemically modified zeta potential

The flow profiles measured for the PB modified channel are given in Fig. 4A. The curves show a linear change in the EOF velocity along the channel height, together with a quadratic component due to the small hydrostatic head that arises due to the displacement of liquid from the entrance to the exit container. In Fig. 4B the mobility $m_{\mathrm{EO}}(y) = u_{\mathrm{EO}}/E_\infty$ has been plotted as a function of the height in the channel. From the values of $m_{\mathrm{EO}}(-h/2)$ and $m_{\mathrm{EO}}(h/2)$ near the PB coated and the bare glass, respectively, the corresponding surface potentials and charges have been calculated using Eqs. (5,13). They are given in Table 1.

The obtained value for the surface charge on the bare glass wall is in agreement with that measured in an uncoated channel at the same pH: -7.9 ± 0.3 $\mathrm{mC/m}^2$. However, the PB coated glass carries not the expected positive charge as measured in a fully coated channel: $+18 \pm 4$ $\mathrm{mC/m}^2$ (to determine the surface charge in this channel we used the solution displacement method [18, 29]). Actually it carries only a less negative charge compared to the bare glass, because the PB coated glass slides were rinsed in DI water such that most of the PB was washed away. Without excessive rinsing, the polymers from the coated wall redissolve in the electrolyte and will adsorb onto the other wall. As a result, the contrast in surface potential, and so the shear flow, will be destroyed within few minutes.

Table 1: The various electrokinetic parameters of the channel.

Channel	Bottom wall			Upper wall			
	m_{EO}	σ	ψ	m_{EO}	σ	ψ	$\dot{\gamma}/E_\infty$
	($\times$ $10^{-9}\mathrm{m}^2$/Vs)	($\mathrm{mC/m}^2$)	(mV)	($\times$ $10^{-9}\mathrm{m}^2$/Vs)	($\mathrm{mC/m}^2$)	(mV)	($\times$ 10^{-5}m/Vs)
A	36±2	-4.5±0.3	-51±3	58±2	-9.1±0.4	-82±3	68±3
B (V=0V)	59±2	-9.3±0.6	-83±3	39±2	-5.0±0.5	-55±3	91±5
B (V=500V)	59±2	-9.3±0.6	-83±3	34±2	-13.4±0.8*	-48±3	113±6

*: This value deviates due to the applied gate voltage, see text.

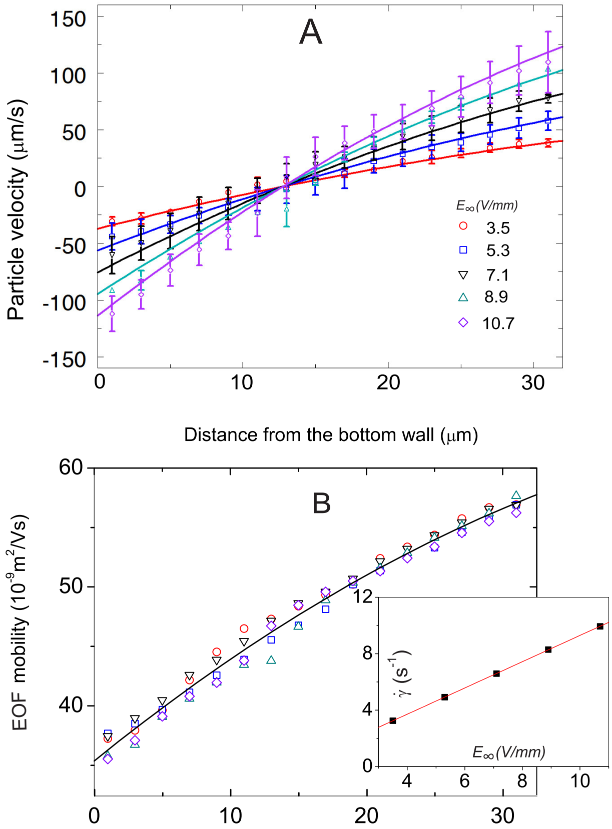

Figure 4: *(A) The particle velocities measured in channel A at different values of E_∞. (B) $m_{\mathrm{EO}}(y) = u_{\mathrm{EO}}/E_\infty$. The inset shows the shear rate versus E_∞.*

By keeping the PB concentration on the coated substrate low, a stable shear profile is maintained for more than ten hours. This is checked by flushing the above channel with water continuously for about ten hours and repeating the flow profile measurements. Comparable stability of multiple PB coating was previously reported. Similarly coated capillaries with PB/DS/PB, Haselberg *et al.* obtained a stability over fifteen hours [19]. Katayama *et al.* reported very stable PB multi layer coatings that endured during 600 replicate analyses and also showed strong stability against 1 M NaOH and 0.1 M HCl [14].

The inset of Fig. 4B shows the shear rate $\dot{\gamma}$ versus the field strength E_∞. The slope of this curve is $(75 \pm 1) \times 10^{-5}$ m/Vs. From Eq. (9) it is clear that this slope must be equal to the magnitude of the slope of m_{EO} versus y (Fig. 4B) which is $(70 \pm 5) \times 10^{-5}$ m/Vs. As argued above the maximum coverage of PB on a single wall is limited, and this sets an upper bound on the charge contrast on opposing walls. So Fig. 4B gives an impression of addressable shear rates. The only way to enhance the shear rate is to decrease the channel height h of this set-up.

4.2 Electrically modified zeta potential

We also modified the surface potential by using an array of gate electrodes as described in Sect. 2.2. In this case the shear rate can be controlled by changing the driving field E_∞ or by varying the gate voltage. Fig. 5 shows the flow profiles measured in channel B, for several driving fields ranging from 2.5 to 12.5 V/mm while the relative gate voltage U was kept at 0 V (panel A) or 500 V (panel B). The corresponding mobilities $m_{\mathrm{EO}}(y)$ for both $U = 0$ V and $U = 500$ V are shown in Fig. 6. The values of the mobility near the lower PDMS wall of the channel, and near the upper wall, i.e. the ONO layer with embedded electrodes, are again used to calculate the corresponding surface charges and potentials which are given in Table 1. Because the surface charge of the ONO layer is lower than that of the PDMS layer, the liquid in the channel is sheared even at 0 V. Fig. 7 shows the measured shear rates as a function of the applied field E_∞. At zero gate voltage, the shear rate per unit field strength is $(88 \pm 5) \times 10^{-5}$ m/Vs, in accordance with the slope of the m_{EO} versus y curve (Fig. 6): $(90 \pm 7) \times 10^{-5}$ m/Vs.

When the relative potential at the gate electrodes is kept at 500 V, the mobility near the upper wall is $+34 \times 10^{-9}$ m^2/Vs. This corresponds to a relative potential at the upper wall of -48 mV, much lower than expected: applying the gate voltage results in a shift of the surface potential by 7 mV. As shown in Fig. 7 the shear rates increase only by about 25 % when the gate voltage is applied. To investigate this in more detail we varied the gate voltage while fixing the driving field at 5 V/mm. The inset of Fig. 7 shows the result. The shear rate seems to saturate at positive gate voltages. We attribute this to saturation of the relative surface potential due to the non linear behavior of the double layer capacitance. In this case the surface potential is determined by both the surface charge and the gate voltage, so we use Eq. (12,13) to calculate the surface charge and we find a decrease from $\sigma = -5$ mC/m^2 to $\sigma = -13$ mC/m^2, see Table 1. So, gate actuation changes the zeta potential only by 0.026 mV/V in contrast to the expected 0.25 mV/V.

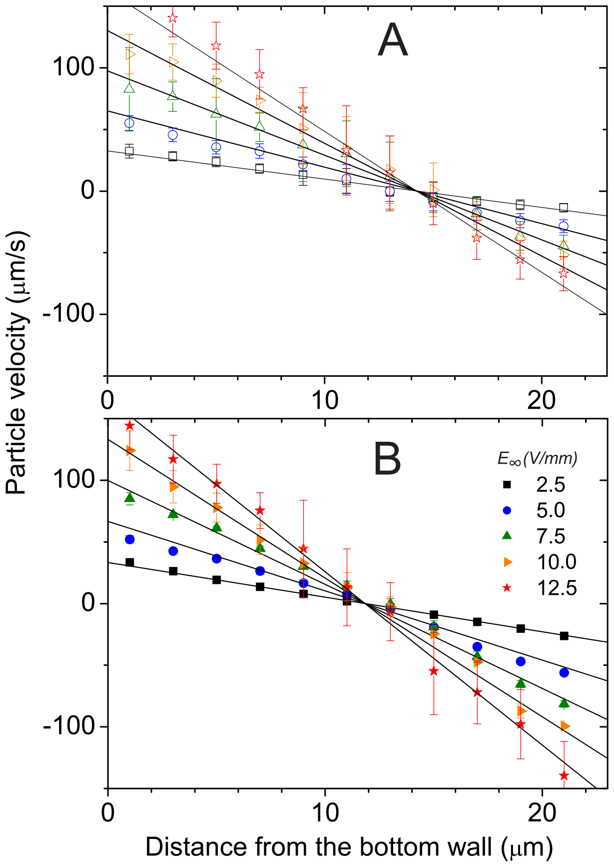

Figure 5: *The particle velocities measured in channel B for several values of* E_∞. *All the data have been fitted in a single linear fit. A)* $V_G = 0$ *V. B)* $V_G = 500$ *V.*

How to explain this much lower value than expected theoretically? We attribute this to charge regulation and the high buffer capacity of the PECVD deposited SiO_2 dielectric layer. This buffer capacity refers to the ability of the layer to resist any pH change near it by dissociating or associating protons. The surface of this dielectric layer contains Silanol groups that can react according: $[\mathrm{SiOH}]_s \leftrightarrow [\mathrm{SiO}^-]_s + [\mathrm{H}^+]_0$ ($pK_1 \simeq 6$) - where $[\ ]_s$ defines a surface density -

and $[\mathrm{SiOH}_2^+]_\mathrm{s} \leftrightarrow [\mathrm{SiOH}]_\mathrm{s} + [\mathrm{H}^+]_0$ ($\mathrm{pK}_2 \simeq -2$), where the proton concentration near the substrate, $[\mathrm{H}^+]_0$, is related to the bulk proton concentration $[\mathrm{H}^+]_\infty$ via the Boltzmann factor: $[\mathrm{H}^+]_0 = [\mathrm{H}^+]_\infty \exp(-\mathrm{e}\psi_\mathrm{s}/\mathrm{k_B T})$. Since the isoelectric point is around $\mathrm{pI} \simeq 2$, the surface will be charged negatively at pH = 3.6. Hence increasing ψ_s (i.e. making ψ_s less negative) implies a decrease of $[\mathrm{H}^+]_0$ and so an increase of the $[\mathrm{SiO}^-]_\mathrm{s}$. Veenhuis *et al.* [27] describe this effect quantitatively in terms of capacitances. When a gate voltage is applied, the surface charge ($\mathrm{C/m^2}$) of the dielectric wall changes due to exchange of protons as

$$\sigma_H = -U_\mathrm{gate} C_{ins} \frac{C_{buff}}{(C_{buff} + C_D)}$$

where C_{buff} is the buffer capacitance of the insulating layer which is proportional to the number of silanol groups on the silicon oxide wall. C_{ins} and C_D are the capacitance of the insulating wall and the double layer, respectively. Considering 4×10^{17} groups/m^2 (approximate value for silicon oxide) we obtain a buffer capacity of 1 F/m^2. Using appropriate values for C_{ins} and C_D, at $U_\mathrm{gate} = 500$ V, we calculate a change in the surface charge of $-12\,\mathrm{mC/m^2}$ which is comparable with the observed change of $-13.4+5 = -8.4\,\mathrm{mC/m^2}$. Hence the observed discrepancy is caused by neglecting this charge regulation effect. See also [32] and [21].

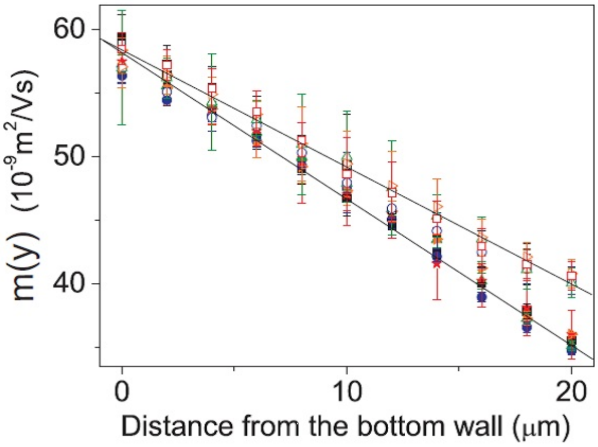

Figure 6: *The function* $m_{EO}(y)$ *for* $V_G = 0$ *V (open symbols) and* $V_G = 500$ *V (filled symbols). The lines are a guide to the eye.*

Moreover, we observed that by applying a negative gate voltage the surface potential can be decreased much more than with a positive voltage, as can be observed from the inset of Fig. 7. However, we also found a very low breakdown voltage when the ONO layers are biased with a negative voltage, so we were not able to study the negative voltage regime. This effect might be due to charge trapping in the layer during PECVD deposition [31].

As discussed in section 2.2, there exist local pressure gradients in the channel due to the inhomogeneity in surface potential along the upper wall. Using Eqs. (15-17), we estimate that these pressure gradients contribute less than 5% to the average EOF velocity. Hence, the linear flow profiles are slightly contaminated by a small parabolic contribution which is of the order of the experimental accuracy (as can be concluded from Fig. 6) and therefore not taken into account in the analysis. The pressure contribution can be further minimized by increasing the number N of gate electrodes while reducing their width w such that the product Nw and ratio $d/w \ll 1$ stay constant.

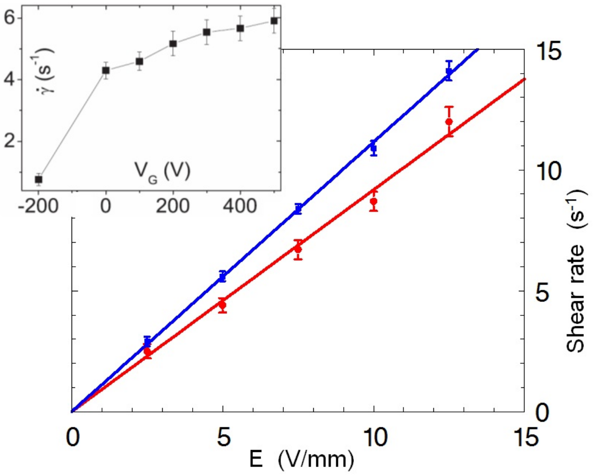

Figure 7: *The shear rates with gate voltage of 0 (red circles) and 500 V (blue squares) versus* E_∞*. The lines are the linear fit. The inset shows the variation of the shear rate with gate voltage at fixed* $E_\infty = 5$ *V/mm.*

The native surface charge on PECVD grown ONO layers slightly differs from sample to sample and is always less than that on glass or PDMS. This is because the SiO_2 layers are grown from the reaction of SiH_4 and N_2O and the prepared layers can contain a very small concentration of some amino groups. Moreover we observed that the surface charge of such PECVD deposited layers is not stable over time. Therefore we flushed the channel with 100 mM NaOH or KOH to activate all surface groups on the wall. We also filled the channel a few minutes before starting the measurements ensuring equilibrium between surface and liquid. Gate actuation of EOF requires high quality dielectric layers covering the electrodes. However, thin PECVD grown layers have mostly a low breakdown voltage when in contact with an aqueous liquid. This is due to the small pinholes, which are typical for PECVD grown layers. (In solid-solid electrode contact or even with ionic liquids the same layers show mostly a high breakdown voltage.) This issue may be solved by using low pressure chemical vapor deposition (LPCVD) to prepare the dielectric layers.

As a consequence, for Newtonian liquids the accuracy in the obtained shear stress is mainly determined by the accuracy of the zeta potential, which in our case is about 10% or a little better. For non-Newtonian liquids also the error in analysis, described in Appendix A should be considered, which can be as big as 25%.

5 Conclusion

We have shown that EOF can be used to create a linear shear flow in a microchannel by chemically modifying the surface charge on one of the channel walls. Unwanted desorption of these chemicals and adsorption on the opposite wall reduces the charge contrast and therewith the shear component of the flow significantly. Therefore only by keeping the concentration of the adsorbed layer low, results in a stable but limited shear component in the flow. Alternatively one can use gate electrodes embedded in the channel wall to modify its surface potential. The SiO_2 dielectric layer deposited on the gate electrodes to isolate them from the liquid in the channel, has a very low negative surface charge compared to glass or PDMS. This property already created a shear flow at zero gate voltage. By modulating the surface charge of this SiO_2 layer with a gate voltage, we were able to increase the shear rate with only 25%. This limited ability to modify the surface potential is attributed to the enhanced proton desorption due to the applied gate voltage. So, although we have shown that EOF can be used for generating a shear flow in microchannels in order to determine in situ the viscosity of the sample liquid, to make this technique useful in microfluidics, further research for chemically inert dielectric layers is required.

Acknowledgement We thank Frieder Mugele for fruitful discussions and acknowledge MicroNed, the Microtechnology Research Programme of The Netherlands, for financial support of project II-B-2.

Appendix A: Flow profile for a non-Newtonian liquid

For non-Newtonian liquids the steady state flow profile in the channel is determined by Eq. (8)

$$\frac{du}{dy} = \mathrm{g}(\tau; c_1..c_n)$$

with $\tau = \tau_0 + \partial_z p\, y + \varepsilon_0 \varepsilon_l E_\infty \phi'(y)$. The function $\mathrm{g}(\tau; c_1..c_n)$ is a generic function with coefficients c_i which have to be determined experimentally. An example is the commonly used, so called power law fluid: $\eta = \eta_c\, |\dot{\gamma}/\dot{\gamma}_c|^{-m}$ and [33]:

$$g(\tau) = \dot{\gamma}_c |\tau/\tau_0|^{m/(1-m)} (\tau/\tau_0) \tag{18}$$

where $\dot{\gamma}_c = c_1$ and $m = c_2$ are the coefficients which should be determined. Usually $0 < m < 1$. The shear stress at the center line of the channel τ_0 can be obtained from the "no slip" boundary condition at the walls, $y = \pm h/2$, which implies:

$$\int_{-h/2}^{h/2} \mathrm{g}(\tau; c_1..c_n)\, dy = 0 \tag{19}$$

This reveals a relation $\tau_0(c_1..c_n)$ at given values for the parameters κ, ψ_a, ψ_b and E_∞. Just for simplicity we assume in the sequel $\partial_z p = 0$. Then the shear stress in Eq. (19) is given by:

$$\tau = \tau_0 + \tau_E \frac{B - A}{1 - (A + B)^2} \tag{20}$$

where $\tau_E = 4\kappa\varepsilon\varepsilon_0 E_\infty k_B T/eZ$ is linear in E_∞. The functions $A(y)$ and $B(y)$ are given by Eq. (5) in section 2.

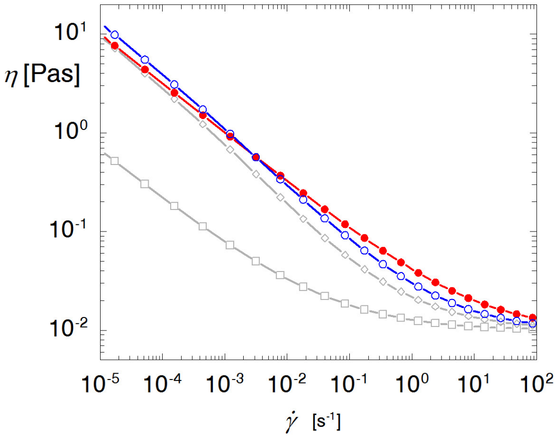

Figure 8: *Comparison of the estimated flow curves from our analysis of $\dot{\gamma}(E_\infty)$ with the true flow curve $\eta(\dot{\gamma})$ (red curve with filled circles). Gray curve with open squares: estimated curve assuming Newtonian behavior of the liquid. Gray curve with open diamonds: first estimate based on the power law index obtained from the experimental $\dot{\gamma}(E_\infty)$ curve. Blue curve with open circles: "best estimate" based on local power law indices obtained from the first estimate.*

To demonstrate how a flow curve $\eta(\dot{\gamma})$ can be obtained we consider a hypothetical fluid that is shear thinning as indicated by the red curve with filled circles in Fig. 8. This hypothetical fluid, with an inverse Debye length κ, flows through our channel due to the surface potentials ψ_a, ψ_b and external field E_∞. We measure the rate of shear at the centerline of the channel, $\dot{\gamma}_0$, as a function of E_∞. The corresponding shear stress at the centerline τ_0 is calculated from κ, ψ_a, ψ_a and E_∞, supposing a certain flow behavior.
If we assume Newtonian behavior (η is constant) $\tau_0^{[N]}$ is given by Eq. (10) and proportional to E_∞. The corresponding flow curve $\eta^{[N]}(\dot{\gamma})$ is obtained via $\eta^{[N]} = \tau_0^{[N]}/\dot{\gamma}_0$ and is represented by the gray curve with open squares in Fig. 8. This curve significantly deviates from the "true" curve.
However, if we assume local power law behavior, i.e. the power law index m varies with $\dot{\gamma}$, our first estimate for m is obtained from a $\dot{\gamma}_0$ vs E_∞ plot:

$$\frac{1}{1-m^{[1]}} = \frac{dln(\dot{\gamma}_0)}{dln(E_\infty)}$$

With this estimate we calculate $\tau_0^{[1]}(E_\infty)$ using Eqs. (18-20). The resulting flow curve $\eta_0^{[1]} = \tau_0^{[1]}/\dot{\gamma}_0$ is given by the gray curve with open diamonds in Fig. 8. Our "best estimate" is obtained by re-estimating m:

$$m^{[2]}(E_\infty) = -\frac{dln(\eta^{[1]}(\dot{\gamma}_0))}{dln(\dot{\gamma}_0)}$$

and recalculating $\tau_0^{[2]}(E_\infty)$ using Eqs. (18-20), again. This results in the blue curve with open circles in Fig. 8, which resembles the "true" flow curve quite well.

Appendix B: Resistor network for the gate electrodes

Let N gate electrodes are connected through $(N-1)$ resistors R, and a variable resistor R' as shown in Fig. 2. The electric potential inside the channel with length L at the middle of the n^{th} electrode at z_n, due to the field $E_\infty = -V_\infty/L$ is given by

$$\phi_n^\infty = \frac{z_n}{L} V_\infty \tag{21}$$

with

$$\begin{aligned} z_n &= (l' - l - w/2) + n\,(l+w) \\ L &= (l' - l + l'') + N\,(l+w) \end{aligned}$$

where w, l, l' and l'' are defined in Fig. 2. The voltage at the the n^{th} electrode is given by

$$V_n = \frac{(R'-R) + nR}{(R'-R) + NR} V_{tot} \tag{22}$$

To obtain the same relative surface potential ψ_n at all gate regions, the potential difference $U_n = V_n - \phi_n^\infty = U$ should be independent of n. This is achieved by choosing R'/R and V_{tot}/V_∞ such that

$$\begin{aligned} \frac{R'}{R} &= \frac{U}{V_\infty}\left(\frac{l'-l+l''}{l+w} + N\right) + \frac{l'+w/2}{l+w} \\ \frac{V_{tot}}{V_\infty} &= \frac{U}{V_\infty} + \frac{l'-l-w/2+N\,(l+w)}{l'-l+l''+N\,(l+w)} \end{aligned}$$

where V_{tot} is the voltage applied to the resistor network.

References

[1] T. M. Squires, S. R. Quake, Reviews of Modern Physics 77 (2005) 978

[2] B. Ladoux and P.S. Doyle, Europhys. Lett. 52 (2000) 511

[3] A. Ansari, C.M. Jones, E.R. Henry, J. Hofrichter, and W.A. Eaton, Science 256 (1992) 1796

[4] N. Resnick and M. A. Gimbrone, Jr., The FASEB Journal 9 (1995) 874

[5] T. Das, T. K. Maiti and S. Chakraborty, Lab on Chip 8 (2008) 1308

[6] J. M. Thwala, J. W. Goodwin,and P. D. Mills, Langmuir 25 (2009) 12926

[7] L.E. Silbert and J.R. Melrose, J. Rheol. 43 (1999) 673

[8] I. Cohen, T. G. Mason, and D. A. Weitz, Phys. Rev. Lett. 93 (2004) 046001-1

[9] M. Kogan, and M. J. Solomon, Langmuir 26 (2010) 1207

[10] Maria L. Olivares, Luciana Vera-Candioti, Claudio L. A. Berli, Electrophoresis 30 (2009) 1

[11] Nadapana Vasu, Sirshendu De, Colloids and Surfaces A: Physicochem. Eng. Aspects 368 (2010) 44

[12] Aditya S. Khair, Denise E. Posluszny, and Lynn M. Walker, Phys. Rev. E 85 (2012) 016320

[13] B.J. Kirby, E.F. Hasselbrink, Electrophoresis 25 (2004) 187

[14] H. Katayama, Y. Ishihama, and N. Asakawa Anal. Chem. 70 (1998) 5272

[15] Y. Liu, J. C. Fanguy, J. M. Bledsoe, and C. S. Henry, Anal. Chem. 72 (2000) 5939

[16] W. L.W. Hau, D. W. Trau, N. J. Sucher, M. Wong and Y. Zohar, J. Micromech. Microeng. 13 (2003) 272

[17] S. L.R. Barker, D. Ross, M. J. Tarlov, M. Gaitan, and L. E. Locascio, Anal. Chem. 72 (2000) 5925

[18] A. Lenzi, F. Viola, F. Bonotto, J. Frey, M. Napoli, S. Pennathur, Electrophoresis 32 (2011) 3295

[19] R. Haselberg, G. J. de Jong, G. W. Somsen, J. Sep. Sci. 32 (2009) 2408

[20] A. D. Stroock, M. Weck, D. T. Chiu, W. T.S. Huck, P. J.A. Kenis, R. F. Ismagilov, and G. M. Whitesides, Phys. Rev. Lett. 84 (2000) 3314

[21] R. B.M. Schasfoort, S. Schlautmann, J. Hendrikse, A. van den Berg, Science 286 (1999) 942

[22] N. J. Sniadecki, C. S. Lee, P. Sivanesan, and D. L. DeVoe, Anal. Chem. 76 (2004) 1942

[23] E.J. van der Wouden, T. Heuser, D.C. Hermes, R.E. Oosterbroek, J.G.E. Gardeniers, A. van den Berg, Colloids and Surfaces A: Physicochem. Eng. Aspects 267 (2005) 110

[24] Z. Jiang and D. Stein, Langmuir 26 (2010) 8161

[25] H. Y. Wu, C. H. Liu, Sensors and Actuators A 118 (2005) 107

[26] R. Karnik, R. Fan, M. Yue, D. Li, P. Yang, and A. Majumdar, Nano Lett. 5 (2005) 943

[27] R. B. H. Veenhuis, E. J. van der Wouden, J. W. van Nieuwkasteele, A. van den Berg and J. C.T. Eijkel, Lab Chip 9 (2009) 3472

[28] Russel, W. B., Saville, D. A., Schowalter, W. R., Colloidal Dispersions, Cambridge University Press, Cambridge (1989)

[29] D. Mampallil, D. van den Ende, F. Mugele, Electrophoresis 31 (2010) 563

[30] F. Sbalzarini and P. Koumoutsakos, Journal of Structural Biology 151 (2005) 182

[31] A. Boogaard, A.Y. Kovalgin and R.A.M. Wolters, Microelectronic engineering 86 (2009) 1707

[32] J. C.T. Eijkel and A. van den Berg, Chem. Soc. Rev. 39 (2010) 957

[33] R.W. Whorlow, Rheological techniques, Ellis Horwood, London (1992)